# Probing magnetization dynamics in individual magnetite nanocrystals using magnetoresistive scanning tunneling microscopy

Amir Hevroni, Boris Tsukerman, and Gil Markovich*

*School of Chemistry, Raymond and Beverly Sackler Faculty of Exact Sciences and Center for Nanoscience and Nanotechnology, Tel Aviv University, Tel Aviv 69978, Israel*

(Received 6 September 2015; revised manuscript received 2 November 2015; published 16 December 2015)

The magnetization dynamics of individual magnetite nanocrystals was probed by variable-temperature magnetoresistive scanning tunneling microscopy, in which a magnetoresistive junction is formed between the substrate and the magnetic particle under study. By tuning the temperature close to the magnetization blocking of a superparamagnetic particle, the slow magnetization switching of the particle caused fluctuations in the tunnel current passing through the particle, which appeared as telegraph noise in current vs time measurements. Analysis of the current fluctuations yielded estimates for the low local magnetic field sensed by the particle, its magnetic anisotropy energy, and the low limit for the spin-polarization degree of the nanocrystals, which for some particles appeared to be as high as 90%.

DOI: 10.1103/PhysRevB.92.224423 PACS number(s): 75.50.Tt, 75.75.Jn, 75.78.−n, 72.25.−b

## I. INTRODUCTION

Studying magnetic nanostructures using magnetic microscopy techniques has posed a formidable technical challenge, especially for relatively small nanostructures on the 10 nm scale. Electron microscopy-based techniques, either scanning electron microscopy (SEM) based (SEM with polarization analysis [1]) or transmission electron microscopy (TEM) based (Lorentz microscopy [2] or electron holography [3]), are typically capable of imaging magnetization in magnetic nanostructures down to the ∼30–40 nm scale. Spin-polarized scanning tunneling microscopy (SP-STM) is capable of obtaining atomic scale magnetization information, but only for atomically flat magnetic atom monolayers [4,5], and micro-superconducting quantum interference devices (micro-SQUIDs) can obtain magnetization data on small (∼10 nm) magnetic particles but only with dilute samples and only around liquid He temperatures (with the exception of sophisticated tricks to transiently heat such systems) [6].

With the continuous shrinking of magnetic bit size and increase in bit density in patterned magnetic media [7], and potentially in solid state spintronic memories [8], there is growing interest to probe the magnetization of individual magnetic nanostructures with high spatial resolution and at different temperatures.

Superparamagnetism occurs in small-enough nanocrystals (NCs) of a ferromagnetic (ferrimagnetic) material forming a single magnetic domain. In such systems, even when the temperature is below the Curie or Néel temperature, the thermal energy is sufficient to change the magnetization direction of an entire particle. The resulting fluctuations in the magnetization orientation cause the NCs' ensemble magnetization to average zero. The material behaves in a manner similar to paramagnetism, except that instead of having individual atom/ion magnetic moment dynamics, the magnetic moment of the entire particle moves as a single giant magnetic dipole [9]. In the absence of an external magnetic field, the characteristic transition time between two magnetic states along an easy axis of magnetization in the particle is presumed to follow the Néel-Brown law [10]:

$$\tau = \frac{1}{f_0}\exp(KV/k_BT) \tag{1}$$

where $f_0$ is the switching attempt frequency (typically of the order of 1–10 GHz for nanometer scale particles [11]), $K$ is the particle's magnetocrystalline anisotropy energy density, $V$ is the particle's volume, $k_B$ is Boltzmann's constant, and $T$ is the temperature. For small-enough magnetic nanoparticles and/or nonspherical particles, the term $KV$ may be replaced by a general magnetic anisotropy energy affected by surface defects and/or particle shape. The switching time depends exponentially on the particle's volume; therefore, for a given temperature, there must be a well-defined particle size at which a transition to stable magnetization occurs for a given sampling rate. For a particle of certain size, there will be a temperature called the blocking temperature, $T_b$, below which the magnetization will be stable over the measurement timescale. Therefore, $T_b$ is dramatically different between particles of different diameters.

The effects of temperature and external magnetic fields on magnetization dynamics in superparamagnetic NC assemblies were previously probed using nanoscale junctions [12]. Tirosh *et al.* [13] had demonstrated an STM-based method that uses spin-dependent tunneling in thin $Fe_3O_4$ (magnetite) NC assemblies to measure the temperature-dependent dynamics of magnetization fluctuations in the NCs. They did so by measuring current changes in time over nanoparticle multilayers at different temperatures. The current fluctuations near $T_b$ closely followed the temperature dependence of the magnetic susceptibility, which was governed by magnetization switching within the nanoparticle array. However, this method could only be used to probe small ensembles of magnetic nanoparticles. Measuring such fluctuations in a single particle is a greater challenge because an additional spin filter electrode is required, either at the tip or at the substrate. Piotrowski *et al.* have recently measured magnetization fluctuations in ∼20 nm magnetite nanoparticles by pinning them on top of a magnetic FePt film, tuning the magnetization switching rate

*gilmar@post.tau.ac.il

 

by an external field, and probing this rate at room temperature through measurement of current fluctuations in a conductive antiferromagnetic (AFM) probe attached to the particles [14]. Recently, relaxation and dephasing measurements of excited nitrogen vacancy (NV) centers in diamonds were also used to probe magnetization dynamics in nearby magnetic nanoparticles [15].

In the present paper, we probed the magnetization dynamics in single magnetite NCs using standard, nonmagnetic PrIr tips by applying a technique we refer to as magnetoresistive (variable-temperature) scanning tunneling microscopy (MR-STM). In MR-STM, the substrate on which the magnetic particles under study are placed acts as the spin filter in place of the tip of SP-STM. The magnetization dynamics would then be probed by placing the tip over a selected particle at a temperature close to its $T_b$ and monitoring the tunneling current over time, where large fluctuations are expected as the particle's magnetization switches, while the substrate's magnetization remains fixed and thus the tunneling probability is expected to change.

To have spin-polarizing properties, the substrate has to be both conductive and magnetic. The choice of materials for the substrate preparation is crucial for several reasons. First, magnetization of the substrate should be in plane to minimize the magnetic field exerted on the deposited particles by the substrate. Second, the substrate surface should be inert to minimize spin scattering at the surface due to oxide formation. Cobalt is known to have a relatively high degree of spin polarization at its Fermi level and tends to form in-plane magnetization domains when in thin film form and the thickness is $>1$ nm [16]. However, its surface readily forms an oxide film in air; therefore, the cobalt layer should be coated with a thin layer of an inert metal, creating a tunnel magnetoresistance (TMR) junction between the particles under study and the substrate. Such an experimental setting is demonstrated by the sketch in Fig. 1. A colloidal magnetite NC would normally have a significant tunnel barrier to the metallic substrate due to surfactant (usually oleic acid) molecules separating the NC and substrate, as well as surface oxidation of $Fe_3O_4$ to $Fe_2O_3$ [17], where the latter has a $\sim$2 eV band gap.

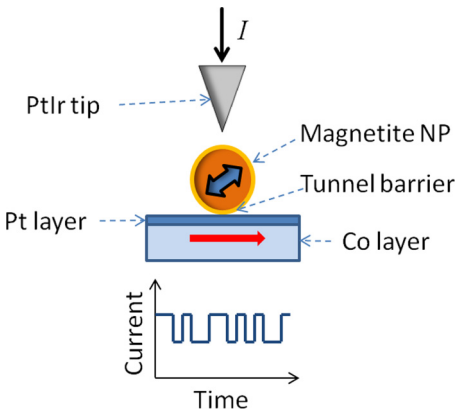


FIG. 1. (Color online) Scheme of the experimental setting. The bias is applied to the tip while the sample is grounded. The temperature is set close to $T_b$ such that the nanoparticle magnetization switches at a kilohertz scale rate.

Another issue crucial for the success of such experiments is the nature of the double barrier tunnel junction (DBTJ) formed in the tip-particle-substrate system. To be affected by the spin polarization within the magnetite NC, the tunnel current has to go through the particle ballistically, without charging the particle. To achieve this situation, the DBTJ has to be asymmetric, where the tip-particle resistance has to be higher than the particle-substrate resistance. This is obtained by keeping the tunnel current low enough and reducing the particle-substrate resistance as much as possible. The experimental evidence of such a situation is the observation of Ohmic current-voltage characteristics for the particle under study (see Supplemental Material [18]). In addition, an asymmetric DBTJ was routinely observed in tip-particle-substrate systems in scanning tunneling spectroscopy (STS) experiments with colloidal semiconductor nanoparticles [19,20].

The last, and probably most important, experimental detail is the choice of magnetite NCs for the experiment. The literature is full of synthesis methods for magnetite, but the produced material may vary in stoichiometry among FeO, $Fe_3O_4$, and $\gamma - Fe_2O_3$ (maghemite). While magnetite and maghemite are both ferrimagnetic compounds with similar saturation magnetization, their electronic structure differs significantly. Magnetite has a nearly zero band gap (probably $\sim$100 meV [21]) with a highly spin-polarized Fermi level, while maghemite is a wide gap semiconductor ($\sim$2 eV [22]). A strong indicator of stoichiometric magnetite is the observation of the Verwey transition [23]. This transition can be detected as a change in conductivity and band gap in magnetite NCs [24,25]. The type of magnetite NCs that were prepared by the coprecipitation method and were used for the present paper have previously been shown to undergo the Verwey transition, as well as significant magnetoresistance (and hence significant spin polarization) [12,13,24]. Conversely, it was shown that syntheses involving high temperature decomposition of iron-organic compounds often leads to nonstoichiometric magnetite [26].

## II. EXPERIMENTAL METHODS

### A. Magnetite NC synthesis

The oleic acid-coated magnetite NCs were synthesized by the coprecipitation method [27]: An aqueous solution containing 2.6 M $FeCl_3$ and 1.3 M $FeCl_2$ (Sigma-Aldrich) was slowly added to $\sim$30 mL of a 25% ammonia solution being vigorously stirred. The procedure was performed under nitrogen atmosphere, at 80°C. Following an equilibration period of $\sim$2 h, the particles were washed several times with distilled water by magnetic decantation. After washing, the aqueous particle precipitate was redispersed in dilute ammonia, excess oleic acid was added, and the dark suspension was stirred for 1 h. Then the suspension was slowly acidified with 1 M HCl until the pH became slightly acidic and an oily black precipitate appeared. The precipitate was dissolved in hexane and reprecipitated by addition of acetone to remove excess, unbound oleic acid. The clean precipitate was separated by centrifugation and dissolved in toluene.

### B. STM sample preparation

A clean $10 \times 10\,\mathrm{mm}^2$Si(001) chip surface with a 100 nm native oxide layer was coated with a 30 nm layer of Co and

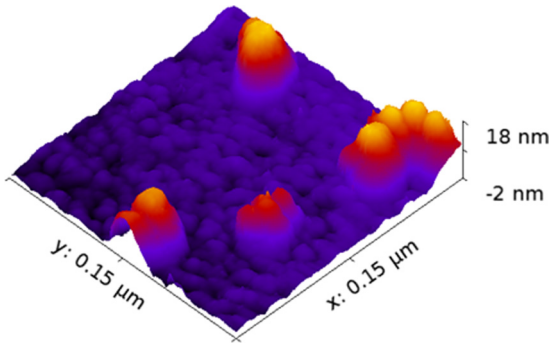


FIG. 2. (Color online) A typical STM topography image of magnetite NCs on a Co/Pt substrate. The imaging was performed under a constant current of $I = 0.1$ nA, and $V = 0.7$ V.

then a 2 nm layer of Pt using electron beam evaporation at rates of 1 and 0.5 Å/s, respectively. The NCs were deposited on the $Si/SiO_2/Co/Pt$ substrate by spin coating of a dilute toluene solution of the NCs.

### C. Characterization

The synthesized NCs were characterized by TEM (Tecnai F20, FEI). The STM sample was characterized by SEM and by superconducting quantum interference device magnetometry (MPMS XL5, Quantum Design). The magnetic characterization consisted of in-plane and out-of-plane magnetization curves and in-plane alternating current (ac) magnetic susceptibility measurements.

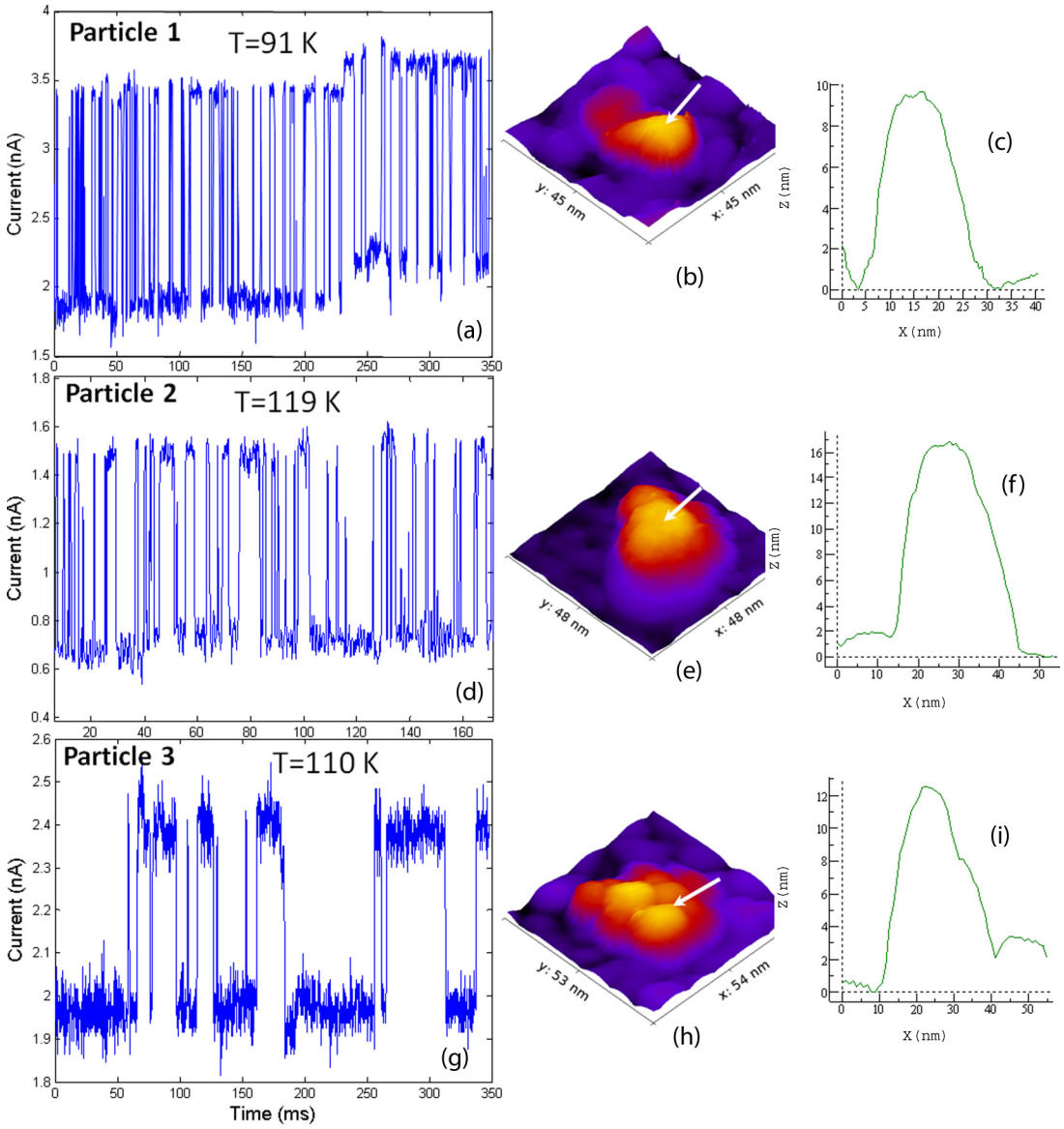


FIG. 3. (Color online) (a), (d), and (g) Current vs time measurements performed on the three particles. Each particle was examined at a different temperature (indicated on the figure). In the case of particle 3, the graph shown is one of five consecutive measurements. (b), (e), and (h) Constant current STM topography images of the three particles. (c), (f), and (i) Height profiles of the measured particles, which are marked by arrows.

### D. STM imaging and $I(t)$ measurements

A $3 \times 9\,\mathrm{mm}^2$ piece of the substrate was cut to fit the STM cooling holder. The STM experiments were performed using an ultrahigh vacuum, variable temperature STM system (Omicron Nanotechnology). To evaporate most of the oleic acid coating off the magnetite NC samples and reduce the particle-substrate resistance, the sample was heated to $\sim 200\,^{\circ}\mathrm{C}$ for several minutes inside the UHV chamber. Hand-cut PtIr tips were used for imaging and measurements. The STM topography images of small areas of the substrates (typically $300 \times 300$ nm) were taken to characterize the sample and make sure that isolated particles or particles within clusters can be identified. Current vs voltage, $I(V)$, and current vs time, $I(t)$, measurements were performed at various temperatures over individual particles, as well as bare Pt areas for control. The sample temperature was controlled by a liquid nitrogen-cooled flow cryostat and could be estimated to an accuracy of $\pm 3$ K by reading the temperature on a diode thermometer attached to the cooling stage. During $I(t)$ measurements, the tip-sample current was kept $\sim$0.1–2.0 nA and the voltage kept $\sim$0.02–0.7 V. In a typical $I(t)$ measurement, after identifying a particle of interest by constant current imaging, the tip was landed over the particle and the current and voltage were adjusted while the feedback was still on to set a particular separation gap between the tip and the particle. The feedback loop was then disengaged, and current values were collected over 160 $\mu$s integration periods with 10 $\mu$s breaks between measurements. A typical $I(t)$ curve consisted of 2048 sampling points, which would take a total of $\sim$350 ms to sample with the 160 $\mu$s integration time.

## III. RESULTS AND DISCUSSION

The magnetization of the substrate was found to be in plane from magnetic hysteresis measurements performed for both in-plane and out-of-plane magnetic fields in a SQUID magnetometer [18]. Therefore, the Co film would exert only minor stray magnetic fields on the deposited NCs due to inhomogeneities in the film. The $\sim$10 nm NCs used for this paper are well within the single magnetic domain regime [28], and similar NCs were previously shown to collectively obey the Néel-Brown relaxation law [29]. The $T_b$ values of the particles were estimated from SQUID ac susceptibility (see Supplemental Material [18]) measurements to be $\sim$100–150 K for most particles, where the imaginary component of the ac magnetic susceptibility seems to peak [18]. The wide range of possible $T_b$ values may be attributed to a broad distribution of particle sizes and the exposure of part of the particles to low magnetic fields from neighboring particles or the substrate.

In typical STM topography scans, the magnetite particles could be easily resolved from the granular metallic background of the substrate, as shown in Fig. 2. This enabled the selection of individual particles on the basis of their size (topography height). Because of the large particle size distribution (and broad relaxation time distribution), it is difficult to predict which particles' magnetization switching rate could be detected by the $I(t)$ measurements at a particular temperature. Namely, at which temperature would the magnetization switching rate of a certain particle be in the kilohertz regime and thus detectable by standard STM electronics? In addition,

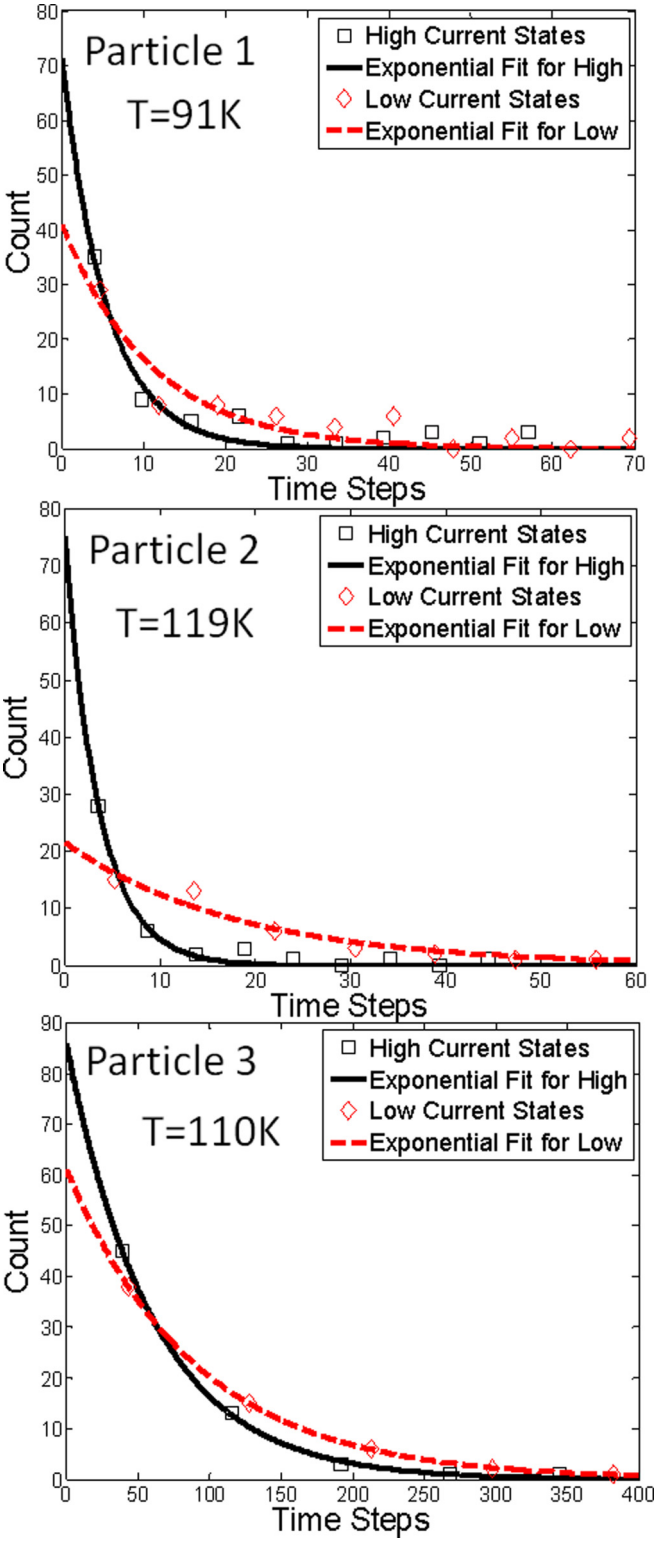


FIG. 4. (Color online) Lifetime distribution histograms of the high and low current states observed for the three particles studied, along with exponential fits to the data.

particles occasionally move around due to interaction with the scanning tip. For these reasons, to make the $I(t)$ measurements fruitful, they were performed during scans as many times and on as many particles as possible, and the data were later analyzed. With the help of STM image analysis programs

TABLE I. Various parameters measured or calculated for the three particles sampled for this paper.

| | Particle 1 | | Particle 2 | | Particle 3 | |
|---|---|---|---|---|---|---|
| | $\tau_- = \tau_{\text{high}}$ | $\tau_+ = \tau_{\text{low}}$ | $\tau_- = \tau_{\text{high}}$ | $\tau_+ = \tau_{\text{low}}$ | $\tau_- = \tau_{\text{high}}$ | $\tau_+ = \tau_{\text{low}}$ |
| $\tau$(ms) | $0.9 \pm 0.3$ | $1.8 \pm 0.6$ | $0.61 \pm 0.16$ | $3.1 \pm 1.2$ | $10.2 \pm 0.9$ | $15.5 \pm 0.5$ |
| $d$(nm) | $10 \pm 1$ | | $16 \pm 1$ | | $12 \pm 1$ | |
| $T$(K) | $91 \pm 3$ | | $119 \pm 3$ | | $110 \pm 3$ | |
| $\mu_0 H$(mT) | $1.7 \pm 0.4$ | | $1.3 \pm 0.2$ | | $0.8 \pm 0.1$ | |
| $K$(J/m$^3$) | $(3 \pm 1) \times 10^4$ | | $(1.1 \pm 0.2) \times 10^4$ | | $(2.7 \pm 0.7) \times 10^4$ | |
| TMR | 84% | | 113% | | 23% | |
| $P_{NP}$ | 74% | | 90% | | 26% | |

(WSxM, Gwyddion [30]), $I(V)$ or $I(t)$ measurements could later be associated with particular particles within topography images. Only particles with roughly Ohmic $I(V)$ behavior, i.e., not charging, were selected for $I(t)$ measurements.

Telegraphic current noise patterns were observed at specific temperatures, both in isolated particles and in particles within clusters, as shown in Fig. 3. The statistical analysis of the magnetization switching events is easier and clearer if one filters the data to remove the low amplitude "white" noise that rides on top of the large amplitude telegraph noise. Hence, the data are binned to two current levels ($I_{\text{bin}}(t)$), low = 0 and high = 1, by applying a threshold current level located between the two states. Occasionally, certain switching $I(t)$ curves would show long pauses in the switching. Such a pause occurred for particle 2 after the first 170 ms; therefore, the data beyond 170 ms were discarded from the analysis.

Binned telegraph current noise data were analyzed for several particles. The simplest analysis is finding the characteristic lifetimes of the high and low current states. Figure 4 presents the high and low state duration statistical distribution for three such particles in the size range of 10–16 nm. Overall, ~10–20 particles exhibited telegraphic $I(t)$ patterns at various temperatures, and we present the three particles that provided a minimal number of current switching events (~50–60) to extract an estimate for the magnetization switching time. The switching time histograms were fitted with an exponential distribution, as shown in Fig. 4, and an estimate for the characteristic magnetization state lifetime was obtained.

A glance reveals that the particles have different levels of asymmetry in high and low current state lifetimes (fitted $\tau_{\text{high}}$ and $\tau_{\text{low}}$; Table I). It is thus clear that the asymmetries in relaxation times reflect asymmetries in the double potential wells representing the magnetization orientation in the particles, which probably originate in an effective local magnetic field experienced by the particles. The projection of this effective field ($\mu_0 H$) onto the easy axis of the particles can be estimated from Néel's law:

$$\tau_{\pm} = \frac{1}{f_0} \exp\left(\frac{KV \pm \mu_0 m H}{k_B T}\right) \tag{2}$$

where $\tau_+$ is the lifetime in the deeper well, $\tau_-$ the lifetime in the shallower well (see Fig. 5 for an illustration), and $m$ is the particle's magnetic moment. In all three particles, it appears that the low current state is the one with the longer lifetime, i.e., corresponding to the lower energy well. This indicates that a particular magnetization orientation of the NCs is favorable with respect to the Co film magnetization. One should also consider the special property of magnetite, where the majority spin population at the Fermi level is spin down, while in the Co substrate it is spin up. Consequently, if one assumes that the NC-substrate barrier does not invert the spin polarization (positive TMR [31]), the plausible possibility is that the stable magnetization orientation of the NCs is closer to parallel with respect to the substrate magnetization, rather than antiparallel. This could be the result of a small out-of-plane magnetic field component of the Co/Pt substrate.

Table I summarizes the local field and magnetic anisotropy energy values extracted by insertion of the various fitted $\tau$ values into the expression in Eq. (2), taking $f_0$ to be 1 GHz and assuming spherical symmetry of the particles' volume with diameter $d$ extracted from their STM topography values. The extracted effective bias field value is of the order of 1 mT for the three particles. This is probably the small out-of-plane field that is produced by imperfections in the cobalt film of the substrate. Two of the three particles have close-neighbor particles, which if blocked during the experimental observation time, would also exert a direct current (dc) bias field on the probed particle. However, apparently, if it exists, this contribution is also fairly small: up to the order of the substrate's stray field.

The extracted $K$ values are all in the $10^4$J/m$^3$ order, and it seems that the larger the particle, the smaller $K$. Around 110 K,

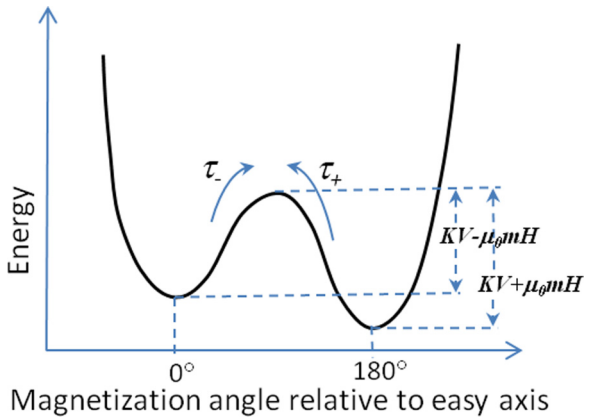


FIG. 5. (Color online) Schematic double potential well representing the magnetic energy of a magnetic particle as a function of the angle between the particle's magnetization orientation and the easy axis in the presence of a small external field with a component $\mu_0 H$ along the easy axis.

bulk magnetite has a magnetocrystalline anisotropy of $\sim 0.5 \times 10^4 \mathrm{J/m^3}$ [32], which is closest to that measured here for particle 2, the largest particle studied. This is reasonable, since the smaller the particle, the more influential other magnetic anisotropy sources, such as shape (deviation from spherical) anisotropy and surface anisotropy, which may overcome the magnetocrystalline anisotropy. Another source of variation in $K$ values between the particles could be its strong dependence on temperature near the Verwey transition, where it inverts the sign due to the change in crystal structure [32]. Thus, the different measurement temperatures and their proximity to the Verwey transition temperature in such particles may lead to differences in $K$ values.

An estimate for the degree of spin polarization in the magnetite nanoparticles studied here could be extracted by using the Julliere model for TMR [33]. The Julliere model for parallel/antiparallel magnetic layers can be summarized by the following equation:

$$\mathrm{TMR} = \frac{G_{\uparrow\uparrow} - G_{\uparrow\downarrow}}{G_{\uparrow\downarrow}} = \frac{I_H - I_L}{I_L} = \frac{2P_S P_{NP}}{1 - P_S P_{NP}} \qquad (3)$$

Consequently, given the spin polarization of the substrate, $P_S$, and the high and low current levels in the telegraphic noise date, $I_H$ and $I_L$, respectively, the particle spin polarization, $P_{NP}$, can be extracted.

Taking the average $I_H$ and $I_L$ values from the $I(t)$ curve of each particle (Fig. 3), we calculated TMR values ranging from 23% (particle 3) to 113% (particle 2). Plugging in a $P_S$ value of bulk cobalt of $\sim$40% [34] yields $P_{NP}$ values ranging between 26% and 90% (Table I). Those are essentially lower limits on the real spin-polarization levels in the particles, as it is assumed in the model that the switching occurs between parallel and antiparallel substrate-particle relative magnetization orientations, which would generally not be the case. This is probably the reason for the large distribution of $P_{NP}$ values among the three particles. The value of 90% spin polarization is remarkably high, probably the highest reported for magnetite NCs, and close to a half-metal electronic configuration [35]. It should be emphasized that the spin-polarization level of the particles is highly dependent on the synthesis method due to the difficulty to achieve proper $Fe^{2+}$: $Fe^{3+}1:2$ stoichiometry. It seems that the traditional coprecipitation method is relatively efficient in obtaining the proper stoichiometry if performed carefully [24,27].

## IV. CONCLUSION

The MR-STM was shown to be an effective method in the detection of superparamagnetic behavior in single domain magnetic nanostructures. The analysis of the telegraph noise $I(t)$ patterns provides a wealth of quantitative information about local magnetic fields acting on the probed particle and the magnetic anisotropy energy, as well as a lower bound estimate for the degree of spin polarization in the NCs. Magnetite NCs were shown to be ideal for this paper, with a $\geqslant$90 % spin polarization confirmed in some of the particles studied.

## ACKNOWLEDGMENTS

The paper was supported by the U.S.–Israel Binational Science Foundation under Grant No. 2010137. The authors gratefully acknowledge useful discussions with Sara Majetich and Stephan Piotrowski.

[1] M. R. Scheinfein, J. Unguris, M. H. Kelley, D. T. Pierce, and R. J. Celotta, Rev. Sci. Instrum. **61**, 2501 (1990).
[2] K. Yamamoto, C. R. Hogg, S. Yamamuro, T. Hirayama, and S. A. Majetich, Appl. Phys. Lett. **98**, 072509 (2011).
[3] R. E. Dunin-Borkowski, T. Kasama, A. Wei, S. L. Tripp, M. J. Hytch, E. Snoeck, R. J. Harrison, and A. Putnis, Microsc. Res. Tech. **64**, 390 (2004).
[4] O. Pietzsch, A. Kubetzka, M. Bode, and R. Wiesendanger, Science **292**, 2053 (2001).
[5] S. Krause, L. Berbil-Bautista, G. Herzog, M. Bode, and R. Wiesendanger, Science **317**, 1537 (2007).
[6] M. Jamet, W. Wernsdorfer, C. Thirion, D. Mailly, V. Dupuis, P. Mélinon, and A. Pérez, Phys. Rev. Lett. **86**, 4676 (2001).
[7] A. O. Adeyeye and N. Singh, J. Phys. D Appl. Phys. **41**, 153001 (2008).
[8] S. Parkin and S. H. Yang, Nat. Nanotechnol. **10**, 195 (2015).
[9] U. Jeong, X. Teng, Y. Wang, H. Yang, and Y. Xia, Adv. Mater. **19**, 33 (2007).
[10] W. F. Brown, Phys. Rev. **130**, 1677 (1963).
[11] T. Jonsson, J. Mattsson, P. Nordblad, and P. Svedlindh, J. Magn. Magn. Mater. **168**, 269 (1997).
[12] N. Taub and G. Markovich, J. Phys. D Appl. Phys. **43**, 485003 (2010).
[13] E. Tirosh, B. Tsukerman, N. Taub, S. A. Majetich, and G. Markovich, Phys. Rev. B **80**, 224427 (2009).
[14] S. K. Piotrowski, M. F. Matty, and S. A. Majetich, IEEE Trans. Mag. **50**, 2303704 (2014).
[15] D. Schmid-Lorch, T. Haberle, F. Reinhard, A. Zappe, M. Slota, L. Bogani, A. Finkler, and J. Wrachtrup, Nano Lett. **15**, 4942 (2015).
[16] C. Chappert and P. Bruno, J. Appl. Phys. **64**, 5736 (1988).
[17] R. Frison, G. Cernuto, A. Cervellino, O. Zaharko, G. M. Colonna, A. Guagliardi, and N. Masciocchi, Chem. Mater. **25**, 4820 (2013).
[18] See Supplemental Material at http://link.aps.org/supplemental/10.1103/PhysRevB.92.224423 for additional information on microscopy of the NCs, NCs deposited on substrate, magnetization curves, and $I(V)$ curves.
[19] U. Banin, Y. W. Cao, D. Katz, and O. Millo, Nature **400**, 542 (1999).
[20] E. P. A. M. Bakkers, Z. Hens, L. P. Kouwenhoven, L. Gurevich, and D. Vanmaekelbergh, Nanotechnology **13**, 258 (2002).
[21] J. H. Park, L. H. Tjeng, J. W. Allen, P. Metcalf, and C. T. Chen, Phys. Rev. B **55**, 12813 (1997).
[22] M. Bowker, G. Hutchings, P. R. Davies, D. Edwards, R. Davies, S. Shaikhutdinov, and H. J. Freund, Surf. Sci. **606**, 1594 (2012).
[23] E. J. W. Verwey, Nature **144**, 327 (1939).

[24] P. Poddar, T. Fried, G. Markovich, A. Sharoni, D. Katz, T. Wizansky, and O. Millo, Europhys. Lett. **64**, 98 (2003).
[25] Q. Yu, A. Mottaghizadeh, H. Wang, C. Ulysse, A. Zimmers, V. Rebuttini, N. Pinna, and H. Aubin, Phys. Rev. B **90**, 075122 (2014).
[26] F. X. Redl, C. T. Black, G. C. Papaefthymiou, R. L. Sandstrom, M. Yin, H. Zeng, C. B. Murray, and S. P. O'Brien, J. Am. Chem. Soc. **126**, 14583 (2004).
[27] T. Fried, G. Shemer, and G. Markovich, Adv. Mater. **13**, 1158 (2001).
[28] D. J. Dunlop, J. Geophysical Res. **78**, 1780 (1973).
[29] T. Telem-Shafir and G. Markovich, J. Chem. Phys. **123**, 204715 (2005).
[30] I. Horcas, R. Fernández, J. M. Gómez-Rodríguez, J. Colchero, J. Gómez-Herrero, and A. M. Baro, Rev. Sci. Instrum. **78**, 013705 (2007).
[31] J. M. De Teresa, A. Barthelemy, A. Fert, J. P. Contour, F. Montaigne, and P. Seneor, Science **286**, 507 (1999).
[32] D. T. Margulies, F. T. Parker, and A. E. Berkowitz, J. Appl. Phys. **75**, 6097 (1994).
[33] M. Julliere, Phys. Lett. **54A**, 225 (1975).
[34] M. Getzlaff, J. Bansmann, and G. Schonhense, Solid State Comm. **87**, 467 (1970).
[35] M. Fonin, Y. S. Dedkov, R. Pentcheva, U. Rudiger, and G. Guntherodt, J. Phys. Condens. Matter **19**, 315217 (2007).